ACS OMEGA

http://pubs.acs.org/journal/acsodf

Article

Unravelling the Catalytic Activity of MnO_2, TiO_2, and VO_2 (110) Surfaces by Oxygen Coadsorption on Sodium-Adsorbed MO_2 {M = Mn, Ti, V}

Khomotso P. Maenetja* and Phuti E. Ngoepe

Cite This: *ACS Omega* 2022, 7, 25991−25998

Read Online

ACCESS | Metrics & More | Article Recommendations

ABSTRACT: Metal-air batteries have attracted extensive research interest owing to their high theoretical energy density. However, most of the previous studies have been limited by applying pure oxygen in the cathode, without taking into consideration the effect of the catalyst, which plays a significant role in the oxygen reduction reaction (ORR) and oxygen evolution reaction (OER). Adsorption of oxygen on (110) Na-MO_2 is investigated, using density functional theory (DFT) calculations, which is important in the discharging and charging of Na-air batteries. Adsorption of oxygen on Na/MO_2 was investigated, and it was observed that the catalysts encourage the formation of the discharge product reported in the literature, i.e., NaO_2. The surface NaO_2 appears to have bond lengths comparable to those reported for monomer NaO_2.

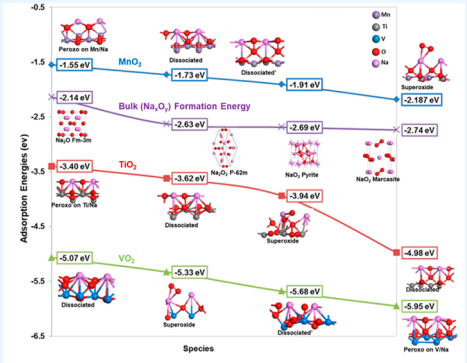

1. INTRODUCTION

Metal-air batteries are ideal for applications where weight is a major consideration. Since oxygen is not stored in the battery, the cathode is much lighter compared to that of a lithium-ion battery. The metal-air battery has the potential of providing energy densities up to three times that of conventional lithium-ion batteries found in electronics devices, not to mention the incoming wave of electric vehicles.[1] It is well-known that Na-air has a lower energy density compared to Li-air batteries;[2−4] thus, we look at the effect of a catalyst in the formation of NaO_2. Lithium oxygen batteries have a theoretical gravimetric energy density of 3456 Wh kg^{-1}, assuming lithium peroxide (Li_2O_2) as the stable discharge product.[5] The theoretical gravimetric energy density of sodium oxygen (Na-O_2) batteries depends on the assumed discharge product and is 1605 Wh kg^{-1} or 1105 Wh kg^{-1} for sodium peroxide (Na_2O_2) or sodium superoxide (NaO_2), respectively. The attention given to sodium-air batteries is due to their high theoretical energy density but also because sodium is an abundant resource.[6] The known discharge products in Na-air batteries are shown in the following equations:

$$Na + O_2 \rightarrow NaO_2;\ E^o = 2.27\ V \quad (1)$$

$$Na + O_2 \rightarrow Na_2O_2;\ E^o = 2.33\ V \quad (2)$$

Conversely, in a Na-air, the formation of the discharge products NaO_2 and Na_2O_2 competes due to the equilibrium potentials of 2.27 and 2.33 V, respectively shown in eqs 1 and 2. Importantly, Kang et al. concluded from computation that Na_2O_2 is more stable in the bulk phase, whereas NaO_2 is more stable at the nanoscale.[7] Although both the peroxide[8,9] and superoxide[10,11] have been reported as the discharge products of a Na-O_2 battery, which discharge product is favored is still not understood. The formation of NaO_2 may be kinetically preferred due to the requirement of only a one-electron transfer compared to two electrons for Na_2O_2.

In the absence of an oxygen evolution reaction catalyst, sodium-air batteries have a cycle life of 80 cycles; after an alloy catalyst was applied, the charge potential showed a decrease from over 4.0 V to below 2.7 V, resulting in an improved energy efficiency. The cells are cycled based on the reversible formation and decomposition of the discharge product, $Na_2O_2 \cdot 2H_2O$. This is an improvement toward real applications in the field of energy storage of metal-air batteries. The oxygen crossover effect is largely suppressed by replacing the oxygen with air, whereas the dense solid electrolyte interphase formed on the sodium anode further prolongs the cycle life. The increased charge overpotential is likely due to the accumulation of side products on the air electrode to cover the active sites of the catalyst.[12]

Received: October 26, 2021
Accepted: March 4, 2022
Published: July 18, 2022

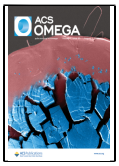

https://doi.org/10.1021/acsomega.1c05990
ACS Omega 2022, 7, 25991−25998

Among transition metal oxides, manganese dioxide has been widely investigated as the catalyst in nonaqueous metal−oxygen batteries, mainly due to its environmental friendliness and easy preparation.[13−15] A question has always been posed as to why MnO_2 is a preferred metal oxide (TiO_2 and VO_2) catalyst in metal-air batteries. To elucidate and gain a better comprehension of this observation, it is necessary to unravel how such a compound, together with other related metal oxides, plays a role in the promotion or inhibition of the growth of dominant discharge products Li_2O_2 or LiO_2 in Li-air batteries, or NaO_2 and Na_2O_2 in Na-air batteries, for example.

Adsorption of oxygen on sodium-adsorbed surfaces was carried out where oxygen atoms were placed in a bulk-like composition, and oxygen molecules were placed in a peroxo form on Na-MO_2. Coadsorption of oxygen was performed in order to simulate the discharge cycle of the metal-air battery whereby oxygen molecules from the atmosphere combine with Na from the anode to form discharge products of Na-air batteries.

Comparison between the metal oxides was investigated in order to validate which of the metal oxides make a better catalyst based on the discharge products' stability and formation, and whether the catalyst encourages formation of the products or not.

2. RESULTS

2.1. Oxygen Adsorption on MO_2 Surfaces. To discuss the redox properties of MO_2's (110) surface, we calculated the adsorption energies of various stoichiometries. We only took into account variations in the oxygen content (the number of M atoms is fixed). If we stick to bulk-like oxygen positions, there are five possible values of = 0 (stoichiometric surface), = 1 and 2. Total oxidation refers to the addition of a full layer of oxygen ions generating manganyl-like, titanyl ,and vanadyl terminations on top of the previously unsaturated M sites. "Mono-peroxo" and "bridging-peroxo" modes of O_2 adsorption[16] are shown in Figure 1.

The oxygen adsorption energies for MnO_2 have been discussed previously discussed in detail[16] together with those on the VO_2 (110) surface.[17] The adsorption energy of an oxygen atom on a five-fold coordinated Ti site (where $\Gamma = 1$) yielded 2.41 eV. When compared to other configurations, the configuration with $\Gamma = 2$ has more electron transfer from the titanium atom to the adatom.

The calculated adsorption energy obtained in this configuration is 0.69 eV and implies that oxidation of the surface has undergone an endothermic process; hence, it is thermodynamically unfavorable. We further adsorbed oxygen as bridging-peroxo unit (O_2^{2-}), split between two Ti surface cations, which requires the least charge transfer per Ti cation of all oxidation possibilities. The mononuclear configuration gives the adsorption energy of 0.070 eV, and the bridging configuration gives 0.37 eV; these values show that the processes are endothermic, which implies a nonspontaneous process shown in Table 1. The mononuclear configuration is energetically most stable configurations where the oxygen molecule is adsorbed in different orientations. The adsorption energies shown in Table 1 reveal that VO_2 adsorbs oxygen strongly[17] both in the form of an atom or molecule.

2.2. Adsorption of Oxygen on Na/MO_2 (110) Surface. We then interrogated the impact of MnO_2, TiO_2, and VO_2 catalysts on the formation of NaO_2 and Na_2O_2, during the cycling of Na-air batteries. Figure 2 shows structures of

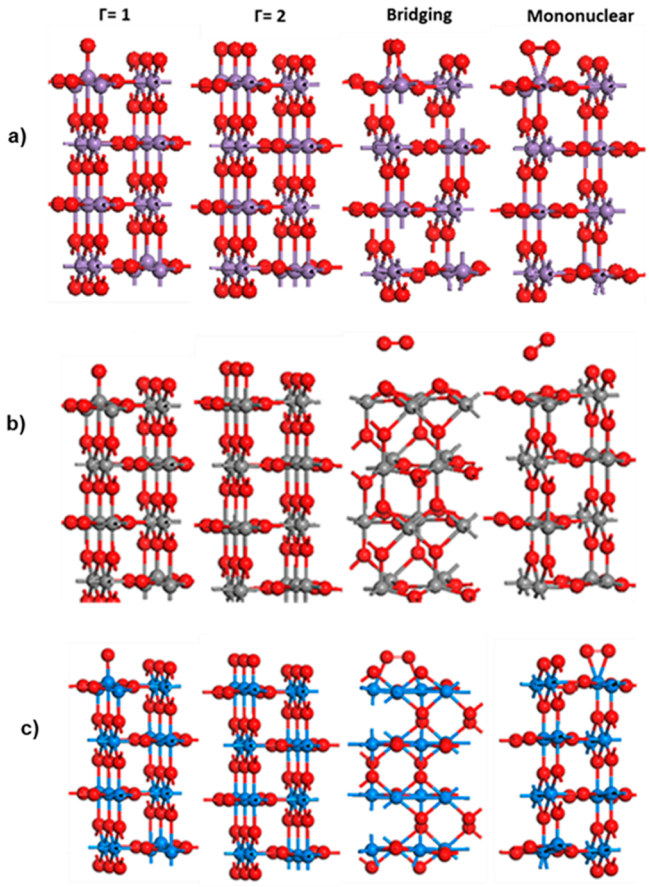

Figure 1. MO_2 (110) (a) MnO_2, (b) TiO_2, and (c) VO_2 with different amounts of surface oxygen. $\Gamma = 1$ and 2 are the partially and totally oxidized surfaces; the bridging and mononuclear peroxo compositions.

Table 1. Adsorption Energies with Different Amounts of Oxygen Adsorbed Surfaces of MO_2

number of oxygens and configuration	MnO_2 Ads energy (eV)[16]	TiO_2 Ads energy (eV)	VO_2Ads energy (eV)[17]
$\Gamma = 1$	1.36	2.41	−2.10
$\Gamma = 2$	1.16	0.67	−1.56
bridging	−1.56	0.37	−3.28
mononuclear	−0.02	−0.07	−3.30

possible discharge products and their related O−O separations, i.e., bulk NaO_2 in pyrite (1.34 Å), marcasite (1.28 Å), $Fm\bar{3}m$ polymorphs, and the corresponding NaO_2 monomer (1.43 Å). Moreover, the bond lengths of O−O in the bulk (1.49 Å) and monomer (1.56 Å) Na_2O_2 are depicted. A variety of oxygen adsorption configurations have been investigated, with some assuming molecular bonding and others assuming dissociative adsorption. Figure 3 depicts four different stable configurations that have been discovered.

The first considered configuration is where one oxygen atom is directly located on top of each Na as a stationary point, which is in fact unstable, since this arrangement subsequently relaxes (if the symmetry of the initial configuration is broken) to a peroxo where two oxygen atoms are bonded to one Na atom, as shown in Figure 3(i). In the superoxide configuration, the oxygen adsorption energy is −2.18 eV/O_2, −3.94 eV/O_2, and −5.33 eV/O_2 for metal oxides surfaces shown in Figure 3. The resulting bond length of 1.29 Å for the O−O associated

https://doi.org/10.1021/acsomega.1c05990
ACS Omega 2022, 7, 25991−25998

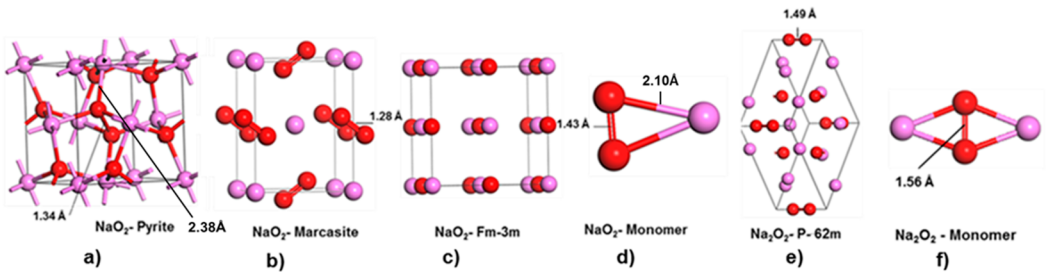

Figure 2. Structures of NaO_2 (a−d) pyrite, marcasite, $Fm\bar{3}m$, and a monomer, respectively, and structures of Na_2O_2; (e, f) $P\bar{6}2m$ and its monomer respectively showing the relaxed O−O distances.[18]

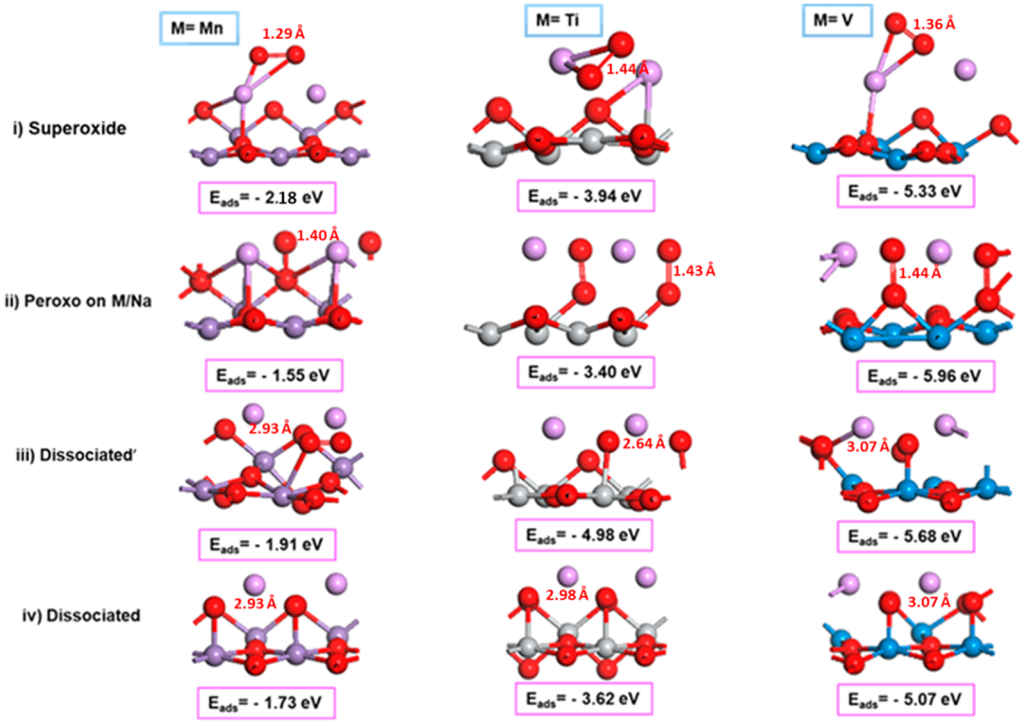

Figure 3. (i−iv) Various configurations that can be adopted by Na−O_2 peroxos when oxygen is adsorbed on different sodiated metal oxide surfaces.

with the MnO_2 catalyst is consistent with those of the bulk marcasite phase of NaO_2. Furthermore, this configuration is the most stable for all MnO_2-based catalysts. For NaO_2, the bond length of 1.44 Å (O−O) induced by the TiO_2 catalyst is consistent with that of the NaO_2 (1.43 Å) monomer and is the second most stable configuration for TiO_2. However, the bond length of (O−O) in NaO_2 where VO_2 is the supporting catalyst compares well with the bond length (O−O) in the pyrite form of NaO_2, which is 1.34 Å, and it is the least stable configuration.

The Na-peroxo adsorption configuration is not the only stable peroxo adsorption configuration: a peroxo group perpendicular to the surface and binding to Na on one end and to M on the other end, as in Figure 3(ii) (E_{ads} = −1.55 eV/O_2, −3.40 eV/O_2, −5.96 eV/O_2 for the metal oxides as they are shown in Figure 3), are stable. In the case of MnO_2 and TiO_2 catalysts such configuration is least stable, whereas for VO_2 it is the most stable arrangement. The molecular form of oxygen is maintained with a bond length ranging from 1.40 to 1.44 Å, which is comparable to the O−O bond length of 1.43 Å in the NaO_2 monomer. The length of such a bond is likewise closer to that of the bulk Na_2O_2, namely, 1.49 Å.

Another configuration occurs when locating oxygens above two previously unsaturated M cations, as in Figure 3(iii). Upon relaxation, the oxygens remain separated with bond lengths ranging from 2.55 to 3.07 Å, mainly suggesting a dissociated configuration, which is, however, stable as shown by the adsorption energies (E_{ads}= −1.91 eV/O_2, −4.98 eV/O_2, −5.68 eV/O_2 for MnO_2, TiO_2, and VO_2 respectively). The configurations in Figure 3(iii) are the second most stable for MnO_2 and VO_2, but for TiO_2, it is the most stable. Figure 3(iv) shows an additional stable dissociative configuration with an oxygen atom on the "bulk-like" positions on top of each of the M cations but with additional bonds formed with the Na adatoms, as in Figure 3(iv) (E_{ads} = −1.73 eV/O_2, −3.62 eV/O_2 and −5.96 eV/O_2). In general, it is the second least stable configuration in Figure 3. Large O−O separations ranging from 2.93 to 3.09 across all metal oxides further confirm the dissociation.

There is no trend in terms of the most stable surface; for MnO_2, the most stable configuration is the peroxo group on sodium, which clearly shows or encourages the formation of NaO_2. The most stable configuration for the adsorption of oxygen on the Na-TiO_2 is the configuration with the peroxo on

https://doi.org/10.1021/acsomega.1c05990
ACS Omega 2022, 7, 25991−25998

Ti, while the most stable configuration for the adsorption of oxygen on Na-VO_2 is the configuration with peroxo on the surface V and adsorbed Na. The adsorption energy for oxygen adsorption on Na-MO_2 is negative, indicating an exothermic reaction that does not require energy to occur and is therefore spontaneous.

The dissociated and peroxo on Ti/Na are the least stable configurations relative to other configurations but still stable compared to pure TiO_2 surface which depicts similar tendencies as MnO_2.

Oxidation on Na/VO_2 is also stable relative to the Na free surface that is shown in Figure 5, which extends to −1 eV and which is 0.9 eV below the threshold of the Na free surfaces. According to the order of the plots, it is observed that the most stable configuration is the peroxo on V/Na followed by the dissociated', whereas the superoxide and the dissociated are the least stable configurations.

All plots for different compositions (Figures 4, 5, and 6) appear to be most stable in all three metal oxides because the

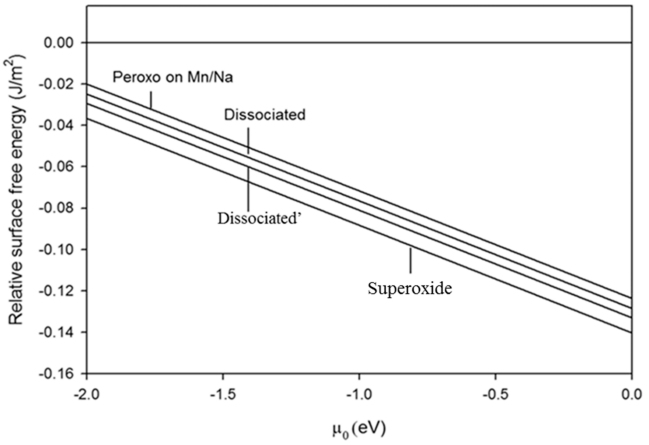

Figure 4. Surface free energies of the oxygen coadsorbed on Na/MnO_2 (110) surfaces with respect to Na/MnO_2 (without oxygen on the surface).

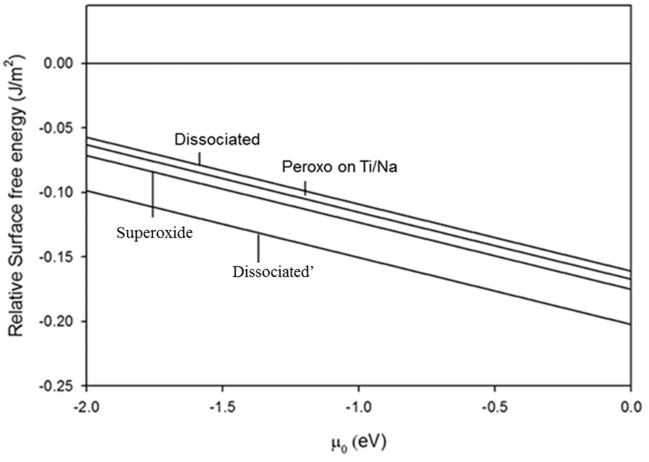

Figure 5. Surface free energies of the oxygen coadsorbed on Na/TiO_2 (110) surfaces with respect to Na/MnO_2 (without oxygen on the surface).

relative surface free energies are negative with a very slight increase in the oxygen chemical potential. The order of

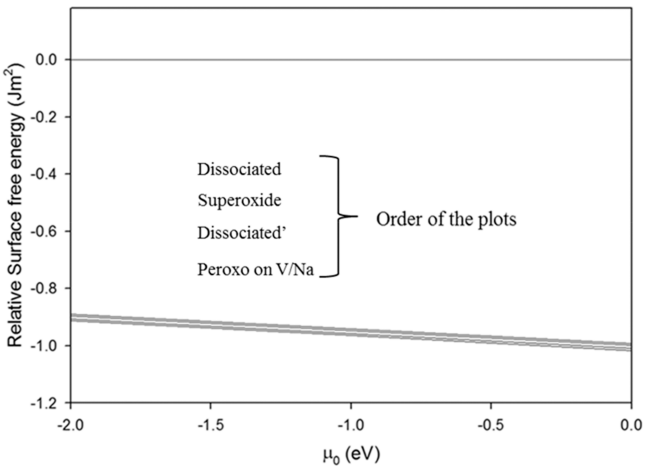

Figure 6. Surface free energies of the oxygen coadsorbed on Na/VO_2 (110) surfaces with respect to Na/MnO_2 (without oxygen on the surface).

stability on the plots is in agreement with the calculated adsorption energies of the oxygen adsorption on Na-MO_2.

3. DISCUSSION

3.1. Effect of Metal Oxide Catalysts in the Cathode Reaction in a Na-Air Battery. Na-air batteries have emerged parallel to the study of Li-air batteries as an alternative, based on the substitution of lithium by sodium, in spite of their lower theoretical energy density, which can exhibit better reversibility and much lower overpotentials compared to lithium-based cells.[19,20] During the battery discharge process, molecular oxygen is reduced in the cathode, in the presence of Na cations and electrons, forming sodium superoxide (NaO_2) particles:

$$O_2 + Na^+ + e^- \rightarrow NaO_2 \quad (3)$$

This is subsequently decomposed upon charging in the reverse reaction ($Na^+ + O_2 + e^- \leftrightarrow NaO_2$). Other less prevalent discharge products such as sodium peroxide (Na_2O_2) and peroxide dehydrate ($Na_2O_2{\cdot}2H_2O$) have been reported.[21−23] This is in contrast to nonaqueous Li-air batteries, where Li_2O_2 was unequivocally identified as the final discharge.

The effects concerned with the MnO_2 (110) surface as a catalyst are summarized in Figure 7. First, three bulk polymorphs, $Fm\bar{3}m$, marcasite, and pyrite, of the Na-O_2 battery superoxide discharge product, NaO_2, are shown in Figure 2, and their respective formation energies are −2.14, −2.69, and −2.74 eV[18,24] with corresponding O−O bond lengths of 3.80, 1.28, and 1.34 Å. A competing discharge product is the peroxo Na_2O_2 (symmetry $P\bar{6}2m$) with a formation energy of −2.63 eV and related O−O bond length of 1.49 Å. Furthermore, it is apparent that energies of formation of bulk marcasite (−2.74 eV) and pyrite (−2.69 eV) NaO_2 are lower than adsorption energies of sodium oxides at the MnO_2 (110) surface for all configurations, i.e., from the least stable (−1.55 eV) to the most stable (−2.18 eV) arrangements. In addition, the energy of the bulk $P\bar{6}2m$ peroxo Na_2O_2 is also lower than those of all MnO_2 surface-catalyzed products, which implies that surface MnO_2 promotes nucleation and formation of the discharge products.

This is consistent with the experimental observation that NaO_2 is the main product of the cathode reaction in Na-air batteries, with some Na_2O_2 as a byproduct (both in the

https://doi.org/10.1021/acsomega.1c05990
ACS Omega 2022, 7, 25991−25998

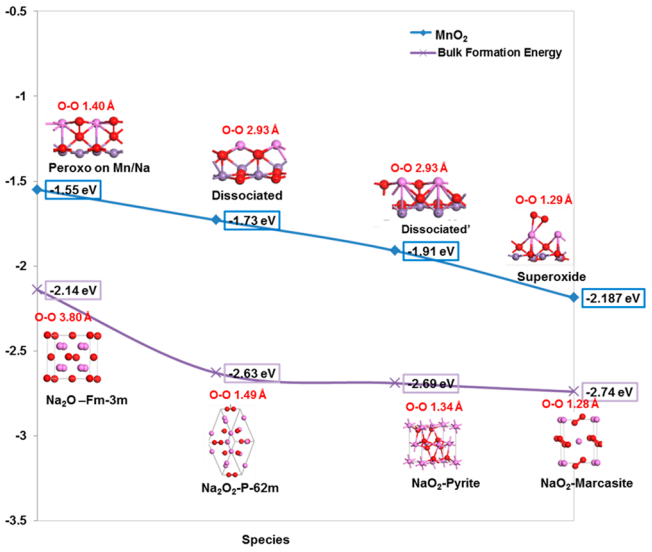

Figure 7. Surface adsorption of MnO_2 (110) and sodium oxide bulk energetics.

presence and in the absence of MnO_2).[19] Indeed, the O−O bond length of the most stable surface configuration (1.29 Å) is nearly equivalent to that of the marcasite (1.28 Å) and not adversely far from one of the pyrite (1.34 Å) phases. On the other hand, the length of the O−O bond of the least stable configuration (1.40 Å) is 6% smaller than that of the bulk phase of the peroxo Na_2O_2. Formation of the dissociated configurations, corresponding to large O−O separations, is also enhanced by the MnO_2 catalyst. All such evidence suggests the MnO_2 catalyst for promoting nucleation and growth of NaO_2 and Na_2O_2 discharge products.

We now consider the TiO_2 (110) surface as a viable catalyst for the formation of NaO_2 products during discharge. A closer look at the energies of formation of bulk NaO_2 polymorphs Na_2O_2 is shown in Figure 8; the energy of formation of the surface sodium oxide at configuration (peroxo on Ti/Na, dissociated, dissociated', and superoxide) indicates that the former (bulk) is higher by 0.93 eV/Na, 2.29 eV/Na, 1.25 eV/

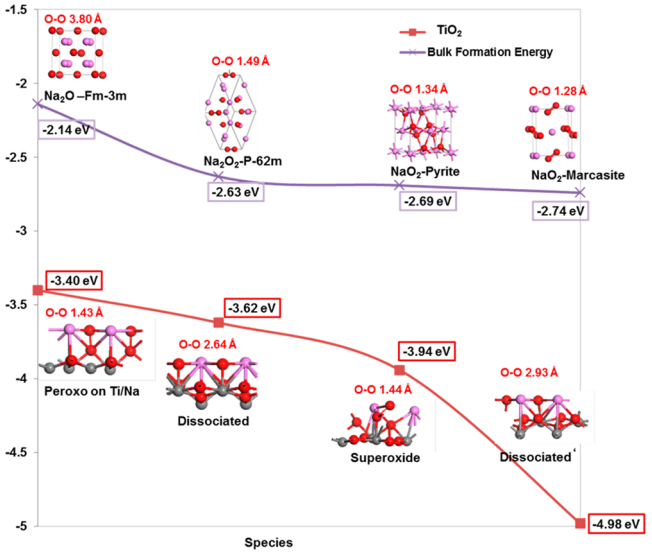

Figure 8. Surface adsorption of TiO_2 (110) and sodium oxide bulk energetics.

Na, and 0.71 eV/Na respectively in all stable configurations for oxygen adsorption on Na-TiO_2 surfaces. This means that the formation of NaO_2 and Na_2O_2 will be discouraged in such configurations because the clusters are too stable and will stick to the surface. In all configurations, the initial reduction of oxygen in the cathode occurs less favorably, i.e., peroxo on Ti/Na, dissociated, and superoxide. Although the energetics do not show the benefit of the TiO_2 (110) surface as a catalyst in the formation of expected discharge products, their associated O−O bond lengths are closer to those of Na_2O_2 bulk and dissociated configurations.

Finally, a comparison of the energy of formation of bulk NaO_2 and Na_2O_2, shown in Figure 9, and the energy of formation of the sodium oxides on the VO_2(110) surface (dissociated, dissociated', superoxide, and peroxo on V/Na) is informative.

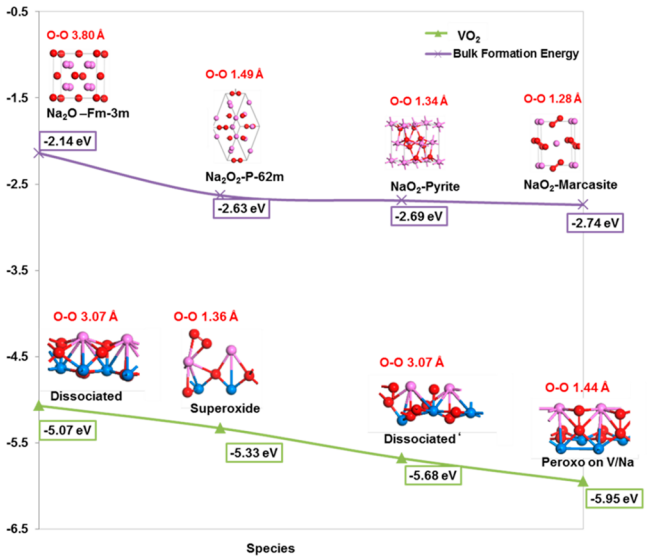

Figure 9. Surface adsorption of VO_2 (110) and sodium oxide bulk energetics.

It indicates that the energy of formation for the bulk is higher compared to those of all stable sodium oxide configurations induced by the VO_2 (110) surfaces. This suggests that formation of NaO_2 and Na_2O_2 will not be enhanced by the VO_2 (110) surface catalyst since the clusters are too stable and would stick to the surface.

Consequently, nucleation and growth of discharge products will not be enhanced by such metal oxides. However, the O−O bond lengths of generated sodium oxides, which are mediated by the catalysts, though not energetically feasible, are closer to those of NaO_2 pyrite (1.36 Å), Na_2O_2 (1.44 Å), and dissociated configurations (3.07 Å).

Similar to rechargeable Li−O_2 batteries, recent studies have alluded to the importance of catalysts in enhancing the performance of Na−O_2 batteries. Carbonaceous materials have been used to accelerate the sluggish behavior of the oxygen reduction reaction (ORR) and oxygen evolution reaction (OER) kinetics in rechargeable Na−O_2.[22,25,26] Although transition metal oxides catalysts have been employed extensively in Li-O_2 batteries,[27−33] owing to the advantages of low cost, high abundance, being environmentally benign, and having considerable catalytic activity in both aqueous and aprotic electrolytes, their use in Na-O_2 batteries is limited.

https://doi.org/10.1021/acsomega.1c05990
ACS Omega 2022, 7, 25991−25998

It has, however, been clearly shown that the porous micro-nanostructured $CaMnO_3$ electrode is an efficient electrocatalyst in Na-O_2 batteries[34] and delivers a high rate capacity and enhanced cyclability. In addition, a composite of $NiCo_2O_4$ nanosheets/Ni foam, as a carbon-free and binder-free electrode for Na-air, has been identified as a highly efficient electrode for nonaqueous Na-air cells. The nanosheets of the discharge products, composed of Na_2O_2 and Na_2CO_3, were observed after discharging in sodium-air batteries.[35] Similarly, our current study has demonstrated that MnO_2, as a catalyst, promotes nucleation and growth of both Na_2O and Na_2O_2. On the contrary, other metal oxides such as TiO_2 and VO_2, do not depict this catalytic effect toward the formation of discharge products in Na-O_2 batteries.

It is further interesting to discuss the current results in light of computations reported by Ceder et al. (2014),[7] which were carried out in the absence of catalysts. They showed that while sodium peroxide (Na_2O_2) is the stable bulk phase of Na in an oxygen environment at standard conditions, sodium superoxide (NaO_2) is considerably more stable at the nanoscale regime. Hence, the superoxide requires much lower nucleation energy than the peroxide, which explains why NaO_2 is reported as the discharge product in some Na-O_2 batteries. Our study proposes that the presence of catalysts, such as the MnO_2 (110) surface, would further lower the nucleation energy for the superoxides and peroxides, and enhance their growth, whereas the TiO_2 and VO_2 would not be effective.

Figure 10 summarizes the surface adsorption and coadsorption of Li and oxygen atoms in comparison to the

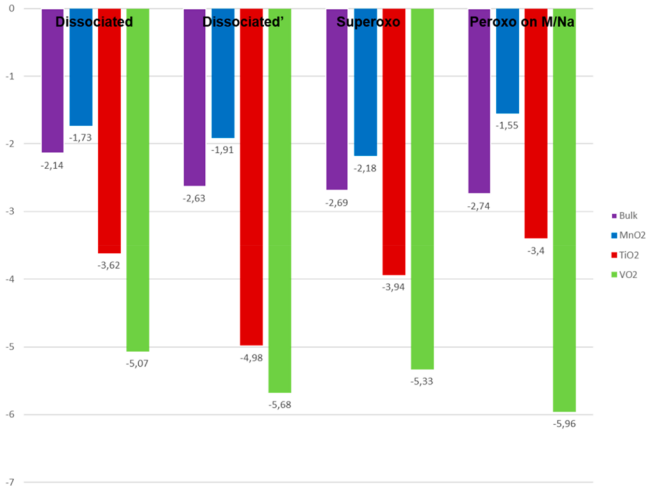

Figure 10. MO_2 surface (110) adsorption and sodium oxide bulk energetics.

formation energies of different bulks of NaO_2 as illustrated in Figures 4–6. This clearly shows the stability of the adsorbed surfaces and the formation energies of the bulk for the metal oxides. The more stable the adsorption energy of the catalyzed systems (compared to the formation energy of the bulk NaO_2), the more unfavorable the configuration, which implies that NaO_2 will stick to the surface, and thus the catalytic property of the metal oxide is not recommended.

4. CONCLUSION

The formation of surface sodium oxide (NaO_2) is more energetically favorable than the formation of gas-phase sodium superoxide (NaO_2) monomers but is less favorable than the formation of NaO_2 bulk, implying that the presence of β-MnO_2 in the cathode of a Na-air battery lowers the energy for the initial reduction of oxygen. In the presence of TiO_2 and VO_2, the formation of the surface NaO_2 is more favorable than the monomer and NaO_2 bulk, which implies that the discharge products will stick to the surface.

For the most stable configurations in the most favored or preferred catalyst, which is MnO_2 in the case for Li-MO_2 and Na-MO_2, it is observed that the stable products predicted are indeed Li_2O_2 and NaO_2, which are observed in the dissociated composition for the Li-MnO_2 surface, while it is the most stable configuration in the Na-MnO_2 surface, which encourages the formation of NaO_2. The discharge products formed in Li-air batteries supported by the metal oxide surface catalyst (MnO_2, TiO_2, and VO_2) have the same bond lengths with their bulk and monomer structures. In summary, in Li-air batteries, that Li_2O_2 is not the only product formed; there is a trace of LiO_2, which is confirmed by the bond length similar to that of the calculated LiO_2 monomer.[33]

The metal oxide catalyst employed in this study (MnO_2, TiO_2, and VO_2) supports the formation of NaO_2 in Na-air batteries, which is the most stable discharge product, and this was supported by the bond length comparison of the clusters (NaO_2) formed with the bulk NaO_2 and NaO_2 monomer calculations.

5. COMPUTATIONAL METHODS

Periodic density functional theory (DFT) computations were carried out using the Vienna Ab initio Simulation Package (VASP) code[36,37] in the form of the Perdew, Burke, and Ernzerhof (PBE) exchange correlation functional[38] in the generalized gradient approximation (GGA). A cutoff kinetic energy of 600 eV was utilized to determine the number of planewaves, and the Monkhorst–Pack Brillouin zone sampling approach with 6 × 6 × 9 and 6 × 6 × 1 k-points mesh for the bulk and surface structures, respectively, was used. We adopted Liechtenstein's nonsimplified rotationally invariant Hubbard correction with the effective Coulomb parameter set U = 2.8 eV and exchange parameter J = 1.2 eV and U = 4.6 eV and exchange parameter J = 0.0 eV.[39,40] The VO_2 calculations were done without the Hubbard correction and were not spin calculations. We first considered the stability of the (110) surface by performing periodic calculations in a slab with stoichiometric composition, thicknesses 14 Å (depending on the oxidation state), and vacuum gaps of ∼14 Å (Figure 1). The two surfaces of each slab are symmetrically equivalent, and this equivalence was kept during all of the calculations, preventing the formation of the electric dipole moments that can be associated with asymmetric slabs.

With variances of roughly +0.8% and −3.1% for a and c, respectively, and 1.6% in the cell volume for the MO_2 indicated in Table 2, the lattice parameters were in good agreement with the experimental results. When the bulk structure was allowed to relax fully and cleaved a (110) surface which was allowed to

Table 2. MnO_2, TiO_2, and VO_2 Bulk Lattice Parameters

structure	a (Å)		c (Å)		V (Å^3)
β-MnO_2	4.366	4.410[41]	2.961	2.887[42]	56.44
β-TiO_2	4.627	4.954[43]	3.008	2.959[41]	64.40
β-VO_2	4.617	4.554[41]	2.774	2.857[42]	59.13

https://doi.org/10.1021/acsomega.1c05990
ACS Omega 2022, 7, 25991−25998

converge as well, and the surface energy was obtained using the expression

$$\gamma = \frac{E_{slab} - E_{bulk}}{2A} \quad (4)$$

where E_{slab} denotes the energy per slab unit cell, E_{bulk} denotes the energy of an equivalent amount of bulk solid, and A is the surface area. The adsorption and coadsorption of sodium and oxygen on clean (110) surfaces are carried out in such a way that stoichiometry and symmetry are maintained throughout the calculations. More information on the methodology can be found elsewhere.[44,45]

$$E_{Ads} = E_{system} - (E_{slab} + E_{adsorbate}) \quad (5)$$

Equatiom 5 is used to calculate the adsorption energy where E_{Ads} is the adsorption energy, E_{system} is the energy of the slab together with its adsorbate, and $E_{adsorbate}$ is the energy of the adsorbate.

AUTHOR INFORMATION

Corresponding Author

Khomotso P. Maenetja − *Materials Modelling Centre, University of Limpopo Private Bag X1106, Sovenga 0727, South Africa;* orcid.org/0000-0002-3199-0946; Email: khomotso.maenetja@gmail.com

Author

Phuti E. Ngoepe − *Materials Modelling Centre, University of Limpopo Private Bag X1106, Sovenga 0727, South Africa*

Complete contact information is available at: https://pubs.acs.org/10.1021/acsomega.1c05990

Notes

The authors declare no competing financial interest.

ACKNOWLEDGMENTS

National Research Foundation for financial assistance and South African Research Chair Initiative of the Department of Science and Technology. The calculations performed at the Centre for High Performance Computing in Cape Town, South Africa; some were performed at our local clusters at Materials Modelling Centre, University of Limpopo, South Africa.

REFERENCES

(1) Abraham, K. M. et al. The Electrochemical Society 217th Meeting Abstract 2010, *0745*, 1.

(2) Adams, B. D.; Radtke, C.; Black, R.; Trudeau, M. L.; Zaghib, K.; Nazar, L. Current density dependence of peroxide formation in the Li−O_2 battery and its effect on charge. *Energy Environ. Sci.* **2013**, *6*, 1772−1778.

(3) McCloskey, B. D.; Bethune, D. S.; Shelby, R. M.; Girishkumar, G.; Luntz, A. C. Solvents' critical role in nonaqueous lithium−oxygen battery electrochemistry. *J. Phys. Chem. Lett.* **2011**, *2*, 1161−1166.

(4) Ottakam Thotiyl, M. M.; Freunberger, S. A.; Peng, Z.; Bruce, P. G. The carbon electrode in nonaqueous Li−O_2 Cells. *J. Am. Chem. Soc.* **2013**, *135* (1), 494−500.

(5) Ha, T. A.; Pozo-Gonzalo, C.; Nairn, K.; MacFarlane, D. R.; Forsyth, M.; Howlett, P. C. An investigation of commercial carbon air cathode structure in ionic liquid based sodium oxygen batteries. *Sci. Rep.* **2020**, *10* (1), 1−10.

(6) Adelhelm, P.; Hartmann, P.; Bender, C. L.; Busche, M.; Eufinger, C.; Janek, J. From lithium to sodium: cell chemistry of room temperature sodium−air and sodium−sulfur batteries. *Beilstein J. Nanotechnol.* **2015**, *6* (1), 1016−1055.

(7) Kang, S. Y.; Mo, Y.; Ong, S. P.; Ceder, G. Nanoscale Stabilization of Sodium Oxides: Implications for Na−O_2 Batteries. *Nano Lett.* **2014**, *14*, 1016−1020.

(8) Sun, Q.; Yang, Y.; Fu, Z. W. Electrochemical properties of room temperature sodium−air batteries with non-aqueous electrolyte. *Electrochem. Commun.* **2012**, *16*, 22−25.

(9) Liu, W.; Sun, Q.; Yang, Y.; Xie, J. Y.; Fu, Z. W. An enhanced electrochemical performance of a sodium−air battery with graphene nanosheets as air electrode catalysts. *Chem. Commun.* **2013**, *49*, 1951−1953.

(10) Hartmann, P.; Bender, C. L.; Sann, J.; Durr, A. K.; Jansen, M.; Janek, J.; Adelhelm, P. A comprehensive study on the cell chemistry of the sodium superoxide (NaO_2) battery. *Phys. Chem. Chem. Phys.* **2013**, *15*, 11661−11672.

(11) McCloskey, B. D.; Garcia, J. M.; Luntz, A. C. Chemical and Electrochemical Differences in Nonaqueous Li−O_2 and Na−O_2 Batteries. *J. Phys. Chem. Lett.* **2014**, *5*, 1230−1235.

(12) Bi, X.; Wang, R.; Yuan, Y.; Zhang, D.; Zhang, T.; Ma, L.; Wu, T.; Shahbazian-Yassar, R.; Amine, K.; Lu, J. From Sodium−Oxygen to Sodium−Air Battery: Enabled by Sodium Peroxide Dihydrate. *Nano Lett.* **2020**, *20* (6), 4681−4686.

(13) Hu, Y.; Zhang, T.; Cheng, F.; Zhao, Q.; Han, X.; Chen, J. Recycling application of Li−MnO_2 batteries as rechargeable lithium−air batteries. *Angew. Chem., Int. Ed.* **2015**, *127*, 4412−4417.

(14) Liu, S.; Wang, G.; Tu, F.; Xie, J.; Yang, H. Y.; Zhang, S.; Zhu, T.; Cao, G.; Zhao, X. Au-nanocrystals-decorated δ-MnO_2 as an efficient catalytic cathode for high-performance Li−O_2 batteries. *Nanoscale* **2015**, *7*, 9589−9596.

(15) Wei, Z. H.; Tan, P.; An, L.; Zhao, T. S. A non-carbon cathode electrode for lithium-oxygen batteries. *Appl. Energy* **2014**, *130*, 134−138.

(16) Mellan, T. A.; Maenetja, K. P.; Ngoepe, P. E.; Woodley, S. M.; Catlow, C. R. A.; Grau-Crespo, R. Lithium and oxygen adsorption at the β-MnO_2 (110) surface. *J. Mater. Chem. A* **2013**, *1* (47), 14879−14887.

(17) Mellan, T. A.; Grau-Crespo, R. Density functional theory study of rutile VO_2 surfaces. *J. Chem. Phys.* **2012**, *137* (15), 154706.

(18) Kang, S.-Y.; Mo, Y.; Ong, P.; Ceder, G. Nanoscale Stabilization of Sodium Oxides: Implications for Na−O_2 Batteries. *Nano Lett.* **2014**, *14*, 1016−1020.

(19) Peled, E.; Golodnitsky, D.; Mazor, H.; Goor, M.; Avshalomov, A. Parameter analysis of a practical lithium- and sodium-air electric vehicle battery. *J. Power Sources* **2011**, *196*, 6835−6840.

(20) Hartmann, P.; Bender, C. L.; Vračar, M.; Dürr, A. K.; Garsuch, A.; Janek, J.; Adelhelm, P. A. A rechargeable room-temperature sodium superoxide (NaO_2) battery. *Nat. Mater.* **2013**, *12*, 228−232.

(21) Li, Y.; Yadegari, H.; Li, X.; Banis, M. N.; Li, R.; Sun, X. Superior catalytic activity of nitrogen-doped graphene cathodes for high energy capacity sodium−air batteries. *Chem. Commun.* **2013**, *49*, 11731−11733.

(22) Kim, J.; Lim, H.-D.; Gwon, H.; Kang, K. Sodium−oxygen batteries with alkyl-carbonate and ether based electrolytes. *Phys. Chem. Chem. Phys.* **2013**, *15*, 3623−36329.

(23) Jian, Z.; Chen, Y.; Li, F.; Zhang, T.; Liu, C.; Zhou, H. High capacity Na−O_2 batteries with carbon nanotube paper as binder-free air cathode. *J. Power Sources* **2014**, *251*, 466−469.

(24) Chase, M. W. *NIST-JANAF Thermochemical Tables*; American Institute of Physics for the National Institute of Standards and Technology: Washington, DC, 1998.

(25) Sun, Q.; Yang, Y.; Fu, Z. W. Electrochemical properties of room temperature sodium−air batteries with non-aqueous electrolyte. *Electrochem. Commun.* **2012**, *16*, 22−25.

(26) Liu, W.; Sun, Q.; Yang, Y.; Xie, J. Y.; Fu, Z. W. An enhanced electrochemical performance of a sodium−air battery with graphene nanosheets as air electrode catalysts. *Chem. Commun.* **2013**, *49*, 1951−1953.

https://doi.org/10.1021/acsomega.1c05990
ACS Omega 2022, 7, 25991−25998

(27) Lin, X.; Shang, Y.; Li, L.; Yu, A. Sea-urchin-like cobalt oxide grown on nickel foam as a carbon-free electrode for lithium−oxygen batteries. *ACS Sustain.Chem. Eng.* **2015**, *3*, 903−908.
(28) Jee, S.; Choi, W.; Ahn, C. H.; Yang, G.; Cho, H. K.; Lee, J.; Yu, C. Enhanced oxygen reduction and evolution by in situ decoration of hematite nanoparticles on carbon nanotube cathodes for high-capacity nonaqueous lithium−oxygen batteries. *J. Mater. Chem. A* **2015**, *3*, 13767−13775.
(29) Zhao, G.; Xu, Z.; Sun, K. Hierarchical porous Co_3O_4 films as cathode catalysts of rechargeable Li-O_2 batteries. *J. Mater. Chem. A* **2013**, *1*, 12862−12867.
(30) Geaney, H.; O'Dwyer, C. Electrochemical investigation of the role of MnO_2 nanorod catalysts in water containing and anhydrous electrolytes for Li−O_2 battery applications. *Phys. Chem. Chem. Phys.* **2015**, *17*, 6748−6759.
(31) Hu, X.; Cheng, F.; Han, X.; Zhang, T.; Chen, J. Oxygen Bubble-Templated Hierarchical Porous ε-MnO_2 as a Superior Catalyst for Rechargeable Li−O_2 Batteries. *Small* **2015**, *11*, 809−813.
(32) Chen, S.; Liu, G.; Yadegari, H.; Wang, H.; Qiao, S. Z. Three-dimensional MnO_2 ultrathin nanosheet aerogels for high-performance Li−O_2 batteries. *J. Mater. Chem. A* **2015**, *3*, 2559−2563.
(33) Maenetja, K. P.; Ngoepe, P. E. First Principles Study of Oxygen Adsorption on Li-MO_2 (M = Mn, Ti and V) (110) Surface. *J. Electrochem. Soc.* **2021**, *168*, 070556.
(34) Hu, Y.; Han, X.; Zhao, Q.; Du, J.; Cheng, F.; Chen, J. Porous perovskite calcium−manganese oxide microspheres as an efficient catalyst for rechargeable sodium−oxygen batteries. *J. Mater. Chem. A* **2015**, *3*, 3320−3324.
(35) Hartmann, P.; Heinemann, M.; Bender, C. L.; Graf, K.; Baumann, R.-P.; Adelhelm, P.; Heiliger, C.; Janek, J. Discharge and Charge Reaction Paths in Sodium-Oxygen Batteries: Does NaO_2 Form by Direct Electrochemical Growth or by Precipitation from Solution? *Phys. Chem. C* **2015**, *119*, 22778−22786.
(36) Kresse, G.; Furthmuller, J. Efficient iterative schemes for ab initio total-energy calculations using a plane-wave basis set. *Phys. Rev.* **1996**, *54*, 11169−11186.
(37) Kresse, G.; Furthmuller, J. Efficiency of ab-initio total energy calculations for metals and semiconductors using a plane-wave basis set. *Comput. Mater. Sci.* **1996**, *6*, 15−50.
(38) Perdew, J. P.; Burke, K.; Ernzerhof, M. Generalized Gradient Approximation Made Simple. *Phys. Rev. Lett.* **1996**, *77*, 3865−3868.
(39) Cockayne, E.; Li, L. First-Principles Studies of the Atomic, Electronic, and Magnetic Structure of α-MnO_2 (Cryptomelane). *Chem. Phys. Lett.* **2012**, *544*, 53−58.
(40) Arroyo-de Dompablo, M. E.; Morales-Garcia, A.; Taravillo, M. DFT+U calculations of crystal lattice, electronic structure, and phase stability under pressure of TiO_2 polymorphs. *J. Chem. Phys.* **2011**, *135*, 054503.
(41) Rogers, K. D. An X-ray diffraction study of semiconductor and metallic vanadium dioxide. *Powder Diffraction* **1993**, *8* (4), 240−244.
(42) Hahn, T. *International Tables of Crystallography, Volume a Space Group Symmetry*, 2nd revised edition; Springer, 1989.
(43) Abrahams, S. C.; Bernstein, J. L. Rutile: Normal Probability Plot Analysis and Accurate Measurement of Crystal Structure. *J. Chem. Phys.* **1971**, *55*, 3206−3211.
(44) Grau-Crespo, R.; Catlow, C. R. A.; De Leeuw, N. H. A computer modeling study of redox processes on the $FeSbO_4$ (100) surface. *J. Catal.* **2007**, *248*, 77−88.
(45) Reuter, K.; Scheffler, M. Composition, structure, and stability of RuO_2 (110) as a function of oxygen pressure. *Phys. Rev. B: Condens. Matter Mater. Phys.* **2001**, *65*, 035406.

https://doi.org/10.1021/acsomega.1c05990
ACS Omega 2022, 7, 25991−25998